sustainability

MDPI

Article

Energy Consumption of the Urban Transport Fleet in UNESCO World Heritage Sites: A Case Study of Ávila (Spain)

Carlos Santos-Iglesia [1], Pablo Fernández-Arias [1], Álvaro Antón-Sancho [2] and Diego Vergara [1,*]

[1] Department of Mechanical Engineering, Catholic University of Ávila, C/Canteros, s/n, 05005 Avila, Spain; carlos.santos@ucavila.es (C.S.-I.); pablo.fernandezarias@ucavila.es (P.F.-A.)
[2] Department of Mathematics and Experimental Science, Catholic University of Ávila, C/Canteros, s/n, 05005 Avila, Spain; alvaro.anton@ucavila.es
* Correspondence: diego.vergara@ucavila.es

Abstract: Emission reduction and energy efficiency are fundamental objectives for the sustainability of the urban transport (UT) sector. One of the actions to achieve these objectives is to replace the vehicles that make up the fleet of UT buses with more efficient ones, equipped with regenerative braking systems that allow the recovery of part of the energy used in travel. However, sometimes the total replacement of the fleet of UT buses is not feasible and only a partial replacement of the fleet is possible. The present study proposes a mathematical model of easy application to compare different UT routes and to locate the greatest improvement niches. The contributions of the proposed model focus on several aspects: (i) optimizing economic resources; (ii) allocating the most efficient equipment where energy consumption can be most optimized; and (iii) simplifying the task of optimizing passenger transport routes. Thanks to the proposed model, the 6 UT lines of the city of Ávila can be classified in order to maximize efficiency in a possible partial renewal of the fleet.

Keywords: energy optimization; energy efficieny; urban transport; Ávila

check for updates

Citation: Santos-Iglesia, C.; Fernández-Arias, P.; Antón-Sancho, Á.; Vergara, D. Energy Consumption of the Urban Transport Fleet in UNESCO World Heritage Sites: A Case Study of Ávila (Spain). *Sustainability* **2022**, *14*, 5641. https://doi.org/10.3390/su14095641

Academic Editor: Marilisa Botte

Received: 22 March 2022
Accepted: 5 May 2022
Published: 7 May 2022

Publisher's Note: MDPI stays neutral with regard to jurisdictional claims in published maps and institutional affiliations.

Copyright: © 2022 by the authors. Licensee MDPI, Basel, Switzerland. This article is an open access article distributed under the terms and conditions of the Creative Commons Attribution (CC BY) license (https://creativecommons.org/licenses/by/4.0/).

1. Introduction

In 2020, the European Commission approved the Sustainable and Intelligent Mobility Strategy, together with an action plan comprising 82 initiatives, grouped into 10 emblematic areas of action, differentiated into 3 dimensions: sustainability, intelligence, and resilience [1,2]. These initiatives, to be developed in the coming years, provide the basis for the European transport system to achieve its transformation towards a more sustainable, inclusive, intelligent, environmentally friendly, and digital transport system.

Given that the transport sector is responsible for a large share of the total greenhouse gas emissions of the European Union (EU), the main objective of this strategy is to be more resilient to future shocks, complying with the Green Deal [3]. In line with the Paris agreement [4], the Green Deal, the EU mechanism for the transformation of the energy system [5] and the development of a green and sustainable economy in a post-COVID-19 scenario [6], has as its main objectives to reduce greenhouse gas emissions by at least 55% from 2025 to 2030 and to reduce greenhouse gas emissions by 90% by 2050, reaching climate neutrality [3,7].

On the other hand, the Framework for Action on Climate and Energy until 2030, to be implemented in the EU as of 2021, includes the following European energy policy objectives for the year 2030: (i) to mandatorily reduce EU greenhouse gas emissions by at least 55%, compared to 1990 values; (ii) to increase the share of renewable energies in total EU energy consumption to at least 32% by the year 2030; and (iii) to improve energy efficiency by at least 32% [8,9].

Among the 82 initiatives developed in the EU Sustainable and Intelligent Mobility Strategy, there is the flagship initiative 2, which aims to boost the adoption of zero emission

vehicles [1,2] and the decarbonization of the transport sector [10]. Within this flagship initiative, road transport is developed, where zero emission solutions are being deployed [11,12]. As of today, manufacturers are investing numerous technical and economic resources in the development of battery electric vehicles [13]. The commercial acceptance of hybrid technology is growing, especially in the case of cars, vans and buses used in urban areas [14–16], while that of long-distance trucks and coaches is beginning to emerge [17,18].

In the Spanish case, transport emissions in 2014 were 77.2 $MtCO_2$-eq, having increased by almost 50% since 1990, due to the increase in the demand for passenger and freight mobility [19–21]. However, since 2007 there has been a decrease in emissions, because of the economic crisis and mitigation measures implemented in this sector [21]. The transport sector accounts for 25% of total greenhouse gas emissions in Spain. Recently, in 2020, the national government approved the Long Term Decarbonization Strategy [21,22].

Finally, in the case of the Castile and Lion region (Spain), in 2009 its regional government approved the Regional Strategy against Climate Change [23], which develops regional policies to mitigate greenhouse gas emissions during this period. Castile and Lion (Figure 1), with an area of more than 90,000 km^2 [24], is the largest region in Spain, even larger than several states which are members of the EU, including Belgium and Portugal.



Figure 1. Geographical location of the city of Ávila (WHS). Own elaboration.

On the other hand, Castile and Lion is one of the regions in the world with the most World Heritage Sites (WHS) declared by UNESCO, with 8 sites: Burgos Cathedral, old town of Segovia and its aqueduct, old town of Ávila with its extra-muros churches, old city of Salamanca, San Millán Yuso and Suso Monasteries (Burgos), the Médulas (León), archaeological site of Atapuerca (Burgos) and prehistoric rock art sites in Siega Verde (Salamanca) [25]. In the case of the region's World Heritage Cities –Ávila, Salamanca, and Segovia–, they include monuments and architectural works of exceptional value, as well as groups of buildings, whether isolated or grouped together, whose architecture, unity and integration into the landscape give them an exceptional universal value from the point of view of history, art, or science.

These WHS cities must specially ensure the protection and conservation of the beauty and history of their urban centers against the effects produced by GHG (greenhouse gases) emissions such as local temperature rise, or changes in the chemical composition of the

atmosphere [26], which eventually lead to rain acidification. To achieve this, they must maintain low levels of atmospheric, noise, light pollution, etc. [27,28]. This indicates that WHS cities should be a priority target for energy sustainability policies. For this reason, it is necessary to carry out energy consumption analyses, particularly in these cities, to help drive these sustainability policies.

Considering this situation, the objective of the present research is to look for energy optimization in the Urban Transport (UT) fleet [29] of one of these WHS cities: Ávila. Regenerative braking systems provide an additional charge to the hybrid batteries while the vehicle is in motion [30–37]. In other words, they take advantage of a large part of the kinetic energy of the vehicle and transform it into electrical energy, which can then be used as a source of energy for the electric motor. The search for energy optimization will consist of finding a method that allows prioritizing the installation of regenerative braking in one line before another, based on energy criteria.

Energy efficiency, as well as the reduction of CO_2 emissions and environmental pollution, must be the criteria to be considered when opting for regenerative technology. The feasibility of this technology would allow the preservation of the monumental wealth of the old town of Ávila, thanks to the reduction of CO_2 emissions from its UT. In the same way, once the viability of this technology is validated, it could be replicated by other fleets of UT buses, favoring the achievement of the desired goal of climate neutrality by the year 2050.

2. Materials and Methods

To develop the present research, a numerical method structured in different phases is developed (Figure 2): Phase I: data acquisition of the different UT routes of the city of Ávila (WHS); Phase II: data processing performing kinematic and dynamic computations; and Phase III: energy analysis determining the supplied power and the recoverable power.

2.1. Phase I: Route Data Collection

To develop Phase I (Figure 2), information is collected from the routes of the 6 passenger UT lines of the city of Ávila [38]. The information collected is based on the number of bus stops and their location along each of the UT lines in the city of Ávila (WHS).

2.2. Phase II: Data Processing

The GPS coordinates of the routes are not publicly available, so it is necessary to do some mapping work to obtain the data of each point of the route (latitude, longitude and altitude) necessary to carry out the study described in this article.

In Phase II (Figure 2), once information is obtained from the transport service provider [38], the route is mapped using the online software Google MyMaps®. Using cartographic techniques [39,40], the complete itinerary is defined, with all the route and stop data, for each of the transport lines included in the study. This information is exported to a file "*.kmz". The application GPSVisualizer® is used to extract all the information contained in the file "*.kmz". The obtained information will be exported in a file "*.txt" containing the hundreds of points that make up the studied route. In addition to the information of the latitude and longitude of each point, the elevation data of each of the points is also available. Once all the information of the coordinates that make up the route is in text, the different parameters of the route are determined (Figure 2).

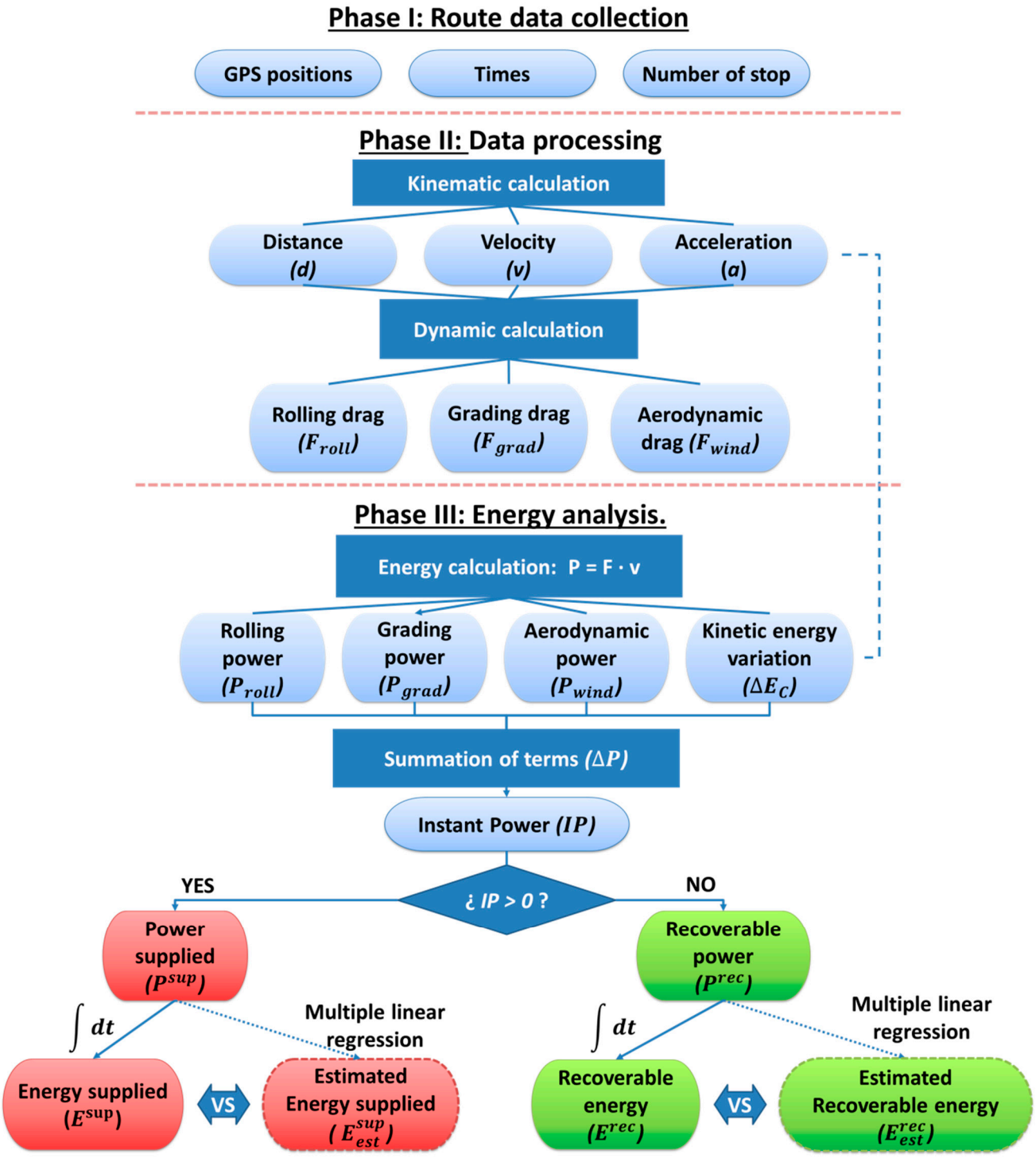


Figure 2. Flowchart of the numeric method.

2.2.1. Kinematic Characteristics

After importing the information, the first step is to compute the distance between two consecutive points on the route (Figure 2). This is calculated by considering the Haversine expression for computing the orthodromic distance between two points on the Earth's crust [41].

At this stage, information is available about the distance between two consecutive points on the route and the cumulative distance between different points. In the same way, it is possible to know the total distance traveled on each route.

From this point, it is possible to obtain what is the distance that the bus must travel to go from one stop to another. This study establishes the starting assumptions that the bus must fulfill along the entire route:

- The bus must be stopped at all bus stops (velocity v = 0 km/h).
- The bus shall not exceed 50 km/h (maximum velocity allowed within the urban area).
- The bus increases its velocity with constant acceleration a corresponding to going from 0 to 50 km/h in 10 s (a = 1.39 m/s^2). The same acceleration value will be used for braking.

With the above starting hypotheses, values are given to the velocity and acceleration functions (Figure 2), both dependent on the variable defined as independent: time. This time-velocity relationship is the one established for different driving cycles widely used for road consumption studies [42–44].

The interval value of the independent variable will be 1 s. Therefore, the average velocities, average accelerations and distance traveled will be calculated for each one-second interval. To comply with the initial hypotheses, the velocity values will decrease sufficiently in advance so that, when the position variable coincides with the distance corresponding to a stop, the velocity variable is equal to zero at that point.

Once the kinematic characteristics of the bus motion are stablished (Figure 2), its technical characteristics can now be defined: (i) Height (H); (ii) Width (W); (iii) Mass (m); (iv) Mass in Running Order (MRO); (v) Maximum Authorized Mass (MAM); (vi) Number of passengers (pax); and (vii) Aerodynamic drag coefficient (C_x) [45], indicated in Table 1.

Table 1. Technical characteristics of the standard bus used for the study.

H (m)	W (m)	MRO (kg)	MAM (kg)	pax	C_x
3.10	2.55	10,000	18,000	86	0.65

In all energy computations, it is assumed that the bus travels the routes considered in each case without any passengers on board. The bus manufacturer does not provide data on the Mass in Running Order (MRO). To compute this data, the mass of the occupants for whom the bus is designed is subtracted from the MAM. The data for the average mass of a passenger is based on the mass of the Humanetics harmonized Hybrid III 50th Male ATD, the world's most widely used automotive test dummy for the evaluation of automotive safety restraint systems in frontal crash tests, which represents the 50th percentile of the population for tests regulated in the US Code of Federal Regulations and in the European ECE Regulations [46]. The mass considered, therefore, for each passenger will be 77.7 kg. Consequently, the computed MRO is:

$$MRO = MAM - (86\ pax \cdot 77.7\ \text{kg}) \quad (1)$$

Finally, the data considered for MRO is rounded to 10,000 kg, to take into account the additional weight of luggage that may be carried by each passenger. As for the aerodynamic drag coefficient, a value of C_x = 0.65 has been taken, a typical value for passenger buses [47].

2.2.2. Dynamic Characteristics

Starting from the bus data (Table 1) and its kinematic behavior, the forces, energies, and powers that occur for each interval of one second along the entire route are computed (Figure 2). To do this, the forces involved are computed for the different situations in which any vehicle moving in a fluid such as air may find itself. In its displacement, the vehicle overcomes 3 forces that oppose its progress: (i) rolling drag; (ii) upward drag and (iii) aerodynamic drag. It should also provide additional energy to accelerate. This energy will be considered as (iv) energy for acceleration.

Firstly, the rolling drag of tires on hard surfaces is mainly due to the concept of hysteresis, which applies to the materials from which the tire is formed [48]. For the

purposes of this research, it is considered that the mentioned moment can be replaced by a horizontal force, of opposite direction to the movement and applied in the center of the wheel [49].

This force is called rolling drag (F_{roll}) (Phase II, Figure 2), it is proportional to mass and gravity, affected by the rolling drag coefficient and then it is expressed in the following form:

$$F_{roll} = m \cdot g \cdot fr \tag{2}$$

where m is mass, g is the Earth gravity acceleration constant, which acts at the center of the wheel, and fr is the so-called rolling drag coefficient [47–52]. If the vehicle is on a slope, the appropriate weight component must be applied. Therefore, the expression of F_{roll} [53] (Phase II, Figure 2) is affected by the cosine of the angle of inclination and it is of the form:

$$F_{roll} = W \cdot fr \cdot \cos \alpha \tag{3}$$

where α is the slope angle.

The fr coefficient is a function of the tire material, its structure, pressure, temperature, tire tread, road roughness, etc. For the computation of vehicle performance, it suffices to consider the fr coefficient as a linear function of velocity. For most vehicle inflation ranges, considering a passenger car driving on a paved road, the following expression is used [47]:

$$fr = 0.01 \cdot \left(1 + \frac{v}{160}\right) \tag{4}$$

where v is the velocity of the vehicle measured in km/h.

On the drag to the ascent, when a vehicle moves up a slope, the vector decomposition of its own weight will produce a component in the longitudinal direction of the vehicle [47,53]. The effect of this component on the longitudinal motion of the vehicle may be to oppose the motion (in the case of a slope with an angle that is $\alpha > 0$) or to assist (in the case when the slope angle is $\alpha < 0$). This slope-related force is often referred to as drag to ascent or grading drag (F_{grad}) (Phase II, Figure 2), which coincides with the weight affected by the sine of the angle of inclination. It is then expressed as follows:

$$F_{grad} = m \cdot g \cdot \sin \alpha \tag{5}$$

The sign criterion used here is that the energy that must be contributed by the motor will have a positive sign and the energy dissipated by the braking systems will be considered with a negative sign. This concept of energy "traditionally dissipated by the braking system" is of vital importance in this study, since it is considered energy that can be used in the case of installing a regenerative braking system. Finally, regarding the aerodynamic drag of the vehicle, it is necessary to consider that a vehicle moving in a fluid (air) experiences a force that resists its forward motion [47,54,55]. This force is called aerodynamic drag (F_{wind}) (Phase II, Figure 2) and is developed in the following expression:

$$F_{wind} = \frac{1}{2} \cdot \rho \cdot Af \cdot C_x \cdot (v - v_w)^2 \tag{6}$$

where ρ is the air density, Af is the frontal area and v_w is the wind velocity.

2.2.3. Energetic Characteristics

Having computed the 3 resisting forces considered in the study (Figure 2), it is easy to compute now the power required to keep the vehicle rolling at a constant velocity by simply multiplying the force by the velocity at each instant [56]. Since the interval of the independent variable is one second, the power terms are equal to the energy terms referring to that interval of one second. Therefore, the rolling power (P_{roll}) (Phase III, Figure 2) is equal to the following:

$$P_{roll} = F_{roll} \cdot v \tag{7}$$

where F_{roll} is the rolling drag, and v is the velocity.

Similarly, the grading power (P_{grad}) (Phase III, Figure 2) coincides with the product of the grading drag times the velocity:

$$P_{grad} = F_{grad} \cdot v \tag{8}$$

where F_{grad} is the grading drag, and v is the velocity.

Based on an analogous reasoning to the previous ones, it follows that the aerodynamic power (P_{wind}) (Phase III, Figure 2) is equal to:

$$P_{wind} = F_{wind} \cdot v \tag{9}$$

where F_{wind} is the aerodynamic drag, and v is the velocity.

Finally, there is a fourth power term to consider. When a vehicle circulates at a constant velocity, it is necessary to provide a power which is equal to the sum of all the powers above, but if the vehicle is accelerated, it is necessary to provide, in addition, certain energy to increase its velocity. This power is not computed as the product of a force with a velocity, but as the difference in kinetic energy between one state and the next divided by the time elapsing between these two states (Phase III, Figure 2). This energy is that corresponding to the increased kinetic energy (ΔE_C), whose expression is well-known:

$$\Delta E_C = \frac{1}{2} m \cdot \Delta v^2 \tag{10}$$

where m is the mass and Δv is the velocity variation between two states. By using time as the independent variable for the computations and discretizing the time variable into one-second intervals, the variation of energy over a one-second interval becomes the definition of power, and, therefore, the increased kinetic energy has units of power, as does P_{roll}, P_{grad} and P_{wind} (Phase III, Figure 2). Once the powers corresponding to the four phenomena considered in the study have been computed for each second (Phase III, Figure 2), the sum of the four power values is calculated, so that a time series of the vehicle's power input or "recoverable" power as a function of time will be obtained. The results shown below are based on the analysis of the energy variations of this time series.

3. Results

Since this study is based on the application of the presented analysis to the city of Ávila, this section presents the most relevant results for the different UT lines of this city (WHS). First, the general results of the orography of the different routes are obtained (Table 2). These results are also represented as profiles of the line (Figure 3), in which the following aspects can be observed: (i) the height at each point along the route; (ii) the slopes that the bus will encounter; (iii) the accumulated slopes; and (iv) the maximum and minimum elevations.

Table 2. Orography of the different UT lines in Ávila (WHS).

UT Line	Total Distance in Each Line (km)	Number of Bus Stops	Cumulative Elevation Gain (m)
1	13.286	45	231.96
2	13.030	48	189.09
3	14.390	47	190.85
4	16.641	50	234.53
5	14.683	46	192.26
6	20.729	65	200.38

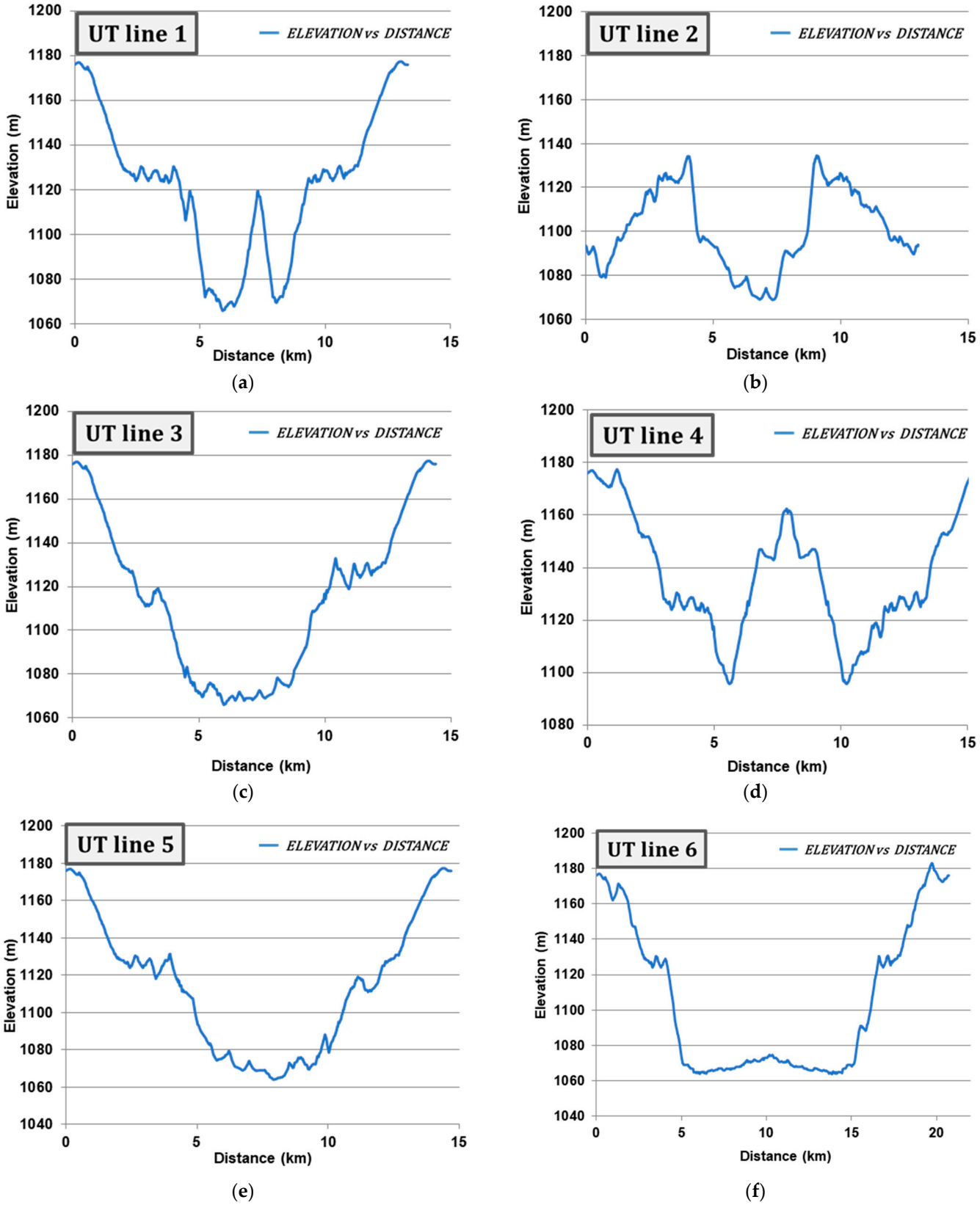


Figure 3. Profile of the different UT lines in the city of Ávila (WHS): (**a**) Line 1; (**b**) Line 2; (**c**) Line 3; (**d**) Line 4; (**e**) Line 5; and (**f**) Line 6.

Since all the distances, heights, and velocities are known, it is possible to compute the Instantaneous Power (*IP*) (Phase III, Figure 2):

$$IP = P_{\text{roll}} + P_{\text{grad}} + P_{\text{wind}} + \Delta Ec \tag{11}$$

To compute *IP*, which is required to supply the vehicle at each moment, it is only necessary to add the power required to maintain the vehicle at a constant velocity and the increase in kinetic energy that the vehicle experiences when changing its velocity in each time interval (in the case of this study, the time interval analyzed is 1 s). The values of P_{roll} and P_{wind} (Phase III, Figure 2) will always be positive for every given velocity v; however, P_{grad} and ΔEc (Phase III, Figure 2) may be positive and oppose the movement of the vehicle [the vehicle is ascending an slope ($P_{\text{grad}} > 0$) or accelerating ($\Delta Ec > 0$)] or negative, favoring the movement [in the case of descending a slope ($P_{\text{grad}} < 0$) or slowing down ($\Delta Ec < 0$)]. In this way, the powers transmitted to the vehicle from the engine, or from the vehicle to the brakes (in case the sum of Equation (11) has a negative value), are known and are plotted in Figure 4.

Figure 4 shows the power values for the six UT lines in the city of Ávila. The positive values of the *IP* variable (red color) that are observed correspond to the power that must be provided to the vehicle to accelerate it or to overcome the resisting forces. The positive values of the *IP* variable are called Supplied Power (P^{sup}) (Phase III, Figure 2).

$$P^{\text{sup}} = |IP|;\ \forall\ IP > 0 \tag{12}$$

The maximum peaks of P^{sup} correspond to the moments when the vehicle accelerates from a standstill at the instant it starts after a stop.

Negative values of *IP* (in green) occur when the result of Equation (11) is negative. These negative values represent an energy input (which would generate an increase in the energy stored in the vehicle if it were equipped with a regenerative braking system). This power, which can be stored in vehicles equipped with regenerative braking systems, is called Recoverable Power (P^{rec}) (Phase III, Figure 2).

$$P^{\text{rec}} = |IP|;\ \forall\ IP \leq 0 \tag{13}$$

It is on this concept of power and recoverable energy that will be worked on below. Each of the peaks with a negative value (green color), is the power necessary to stop the vehicle at the instant in which a deceleration prior to the complete stop of the vehicle is occurring. In conventional vehicles, P^{rec} cannot be harnessed and must be dissipated as heat through the vehicle's conventional braking system.

The remaining power values (positive or negative) are obtained depending on the combination of the aerodynamic force, rolling force, gradient and ΔE_c required to accelerate (Equation (11)). Table 3 shows, as a summary, the results obtained in terms of the Maximum Recoverable Power (kW) and the Average Recoverable Power (kW) in each of the lines under study.

Table 3. Maximum Recoverable Power and Average Recoverable Power (kW) in the different UT lines of Ávila (WHS).

UT Line	Maximum P^{rec} (kW)	Average P^{rec} (kW)
1	264.55	73.29
2	305.37	71.59
3	321.84	67.81
4	278.28	68.74
5	263.50	71.59
6	254.93	75.29

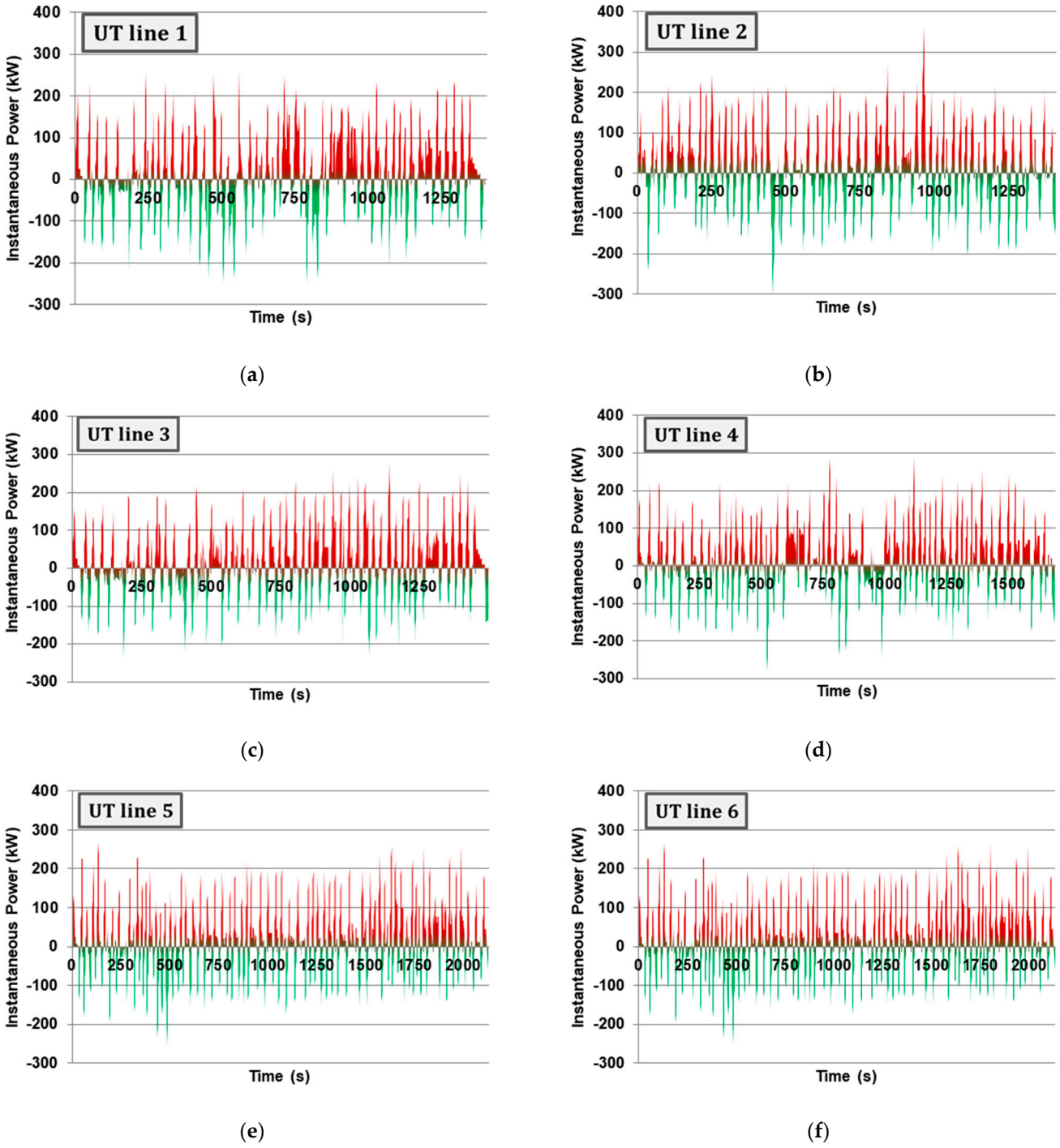


Figure 4. Power distribution of the different UT lines in the city of Ávila (WHS): (**a**) Line 1; (**b**) Line 2; (**c**) Line 3; (**d**) Line 4; (**e**) Line 5; and (**f**) Line 6.

4. Discussion

Once the values of the power with respect to time are known, the energy required to supply the vehicle can be computed by simply integrating the power function over a defined time interval:

$$W = \int P \cdot dt \tag{14}$$

where P is the power.

According to the definition of the integral itself, it can be concluded from the graphs in Figure 4 that the area enclosed under the curve P^{sup} (in red) corresponds to the so-called

Supplied energy (E^{sup}) (Phase III, Figure 2), which is the energy that has been supplied to the vehicle between two specific time instants.

$$E^{\text{sup}} = \int_{P>0} IP \cdot dt \tag{15}$$

Likewise, the area enclosed under the curve P^{rec} corresponds to the Recoverable Energy (E^{rec}) (Phase III, Figure 2) that has been dissipated, but can be used if regenerative braking systems are available.

$$E^{\text{rec}} = \int_{P\leq 0} P \cdot dt \tag{16}$$

In Table 4, the cumulative results for the variables E^{sup} and E^{rec} (Phase III, Figure 2) on each of the UT lines in the city of Ávila (WHS) are computed. However, when evaluating the incorporation of regenerative braking systems, the information provided in Table 4 is not sufficient to study in which lines E^{rec} (Phase III, Figure 2) is greater. In Table 5, the different terms used in this study according to the unit of travel considered (km) is obtained. To compare E^{sup} and E^{rec} (Phase III, Figure 2), regardless of the length of the route, it is necessary to consider relative terms. From the data of Table 5 it is concluded that the amounts of energy required to cover one kilometer of each of the lines are much less than would be expected based on the amounts of energy provided in a complete route. The E^{sup}/km is 12% on the most demanding route (line 2), which is higher than that required to travel one km on line 6. Similarly, it can be observed that the E^{rec} per km on line 2 is 18.5% higher than on line 6.

Table 4. Supplied and recoverable energy (MJ) in the different UT lines of Ávila (WHS).

UT Line	Total E^{sup} in Each Line (MJ)	Total E^{rec} in Each Line (MJ)
1	63.50	44.48
2	63.43	44.95
3	65.87	45.23
4	73.19	49.08
5	66.65	45.46
6	90.14	60.24

Table 5. Number of bus stops, cumulative elevation gain, E^{sup} and E^{rec} (per km traveled) in the different UT lines of Ávila (WHS).

UT Line	Total Distance in Each Line (km)	Relative Results		Relative Energy Results		Percentage of Recoverable Energy (%)
		Number of Stop per km (n°/km) X_1	Cumulative Elevation Gains per km (m/km) X_2	E^{sup} per km (MJ/km)	E^{rec} per km (MJ/km)	
2	13.0305	3.68	14.51	4.87	3.45	70.84
1	13.2861	3.39	17.46	4.78	3.35	70.08
6	20.7292	3.14	9.67	4.35	2.91	66.90
3	14.3902	3.27	13.26	4.58	3.14	68.56
5	14.6833	3.13	13.09	4.54	3.10	68.28
4	16.6416	3.00	14.09	4.40	2.95	67.05

The different transport lines are listed in the table according to their percentage of E^{rec} versus E^{sup} (right column, Table 5). Based on the ratio between E^{rec} and E^{sup}, it can be concluded that the line with the highest percentage of energy that can be recovered is line 2, with 70.87% of E^{sup} recovered. It is important to observe that the scope of this study is to compute the theoretical gross energy available for recovery and that it does not consider either the quality/availability of the energy or the yields that apply to each of the

energy transformations. This is therefore a preliminary study which aims to compare the size of the recoverable energy niches, but it has nevertheless made it possible to classify the lines according to the percentage of recoverable energy. So far, it can be observed that for the same distance traveled, there are significant changes in both E^{sup} and E^{rec}, due to two variables: (i) Number of Bus Stops per km (X_1) and (ii) Cumulative elevation gain per km (X_2). To estimate the contribution of the accumulated difference in elevation and the number of bus stops per kilometer in the overall computation of both E^{sup} and E^{rec}, the following multiple linear regression model is proposed:

$$E_{est}^{sup}(\mathrm{MJ/km}) = 1.296 \cdot X_1 + 0.031 \cdot X_2 \quad (17)$$

$$E_{est}^{rec}(\mathrm{MJ/km}) = 0.826 \cdot X_1 + 0.032 \cdot X_2 \quad (18)$$

where E_{est}^{sup} is the Estimated Supplied Energy and E_{est}^{rec} is the Estimated Recoverable Energy (Phase III, Figure 2). Equation (17) is obtained by means of a multiple linear regression, taking as dependent variable the values of the E^{sup} column, and as independent variable, the X_1 and X_2 values (Table 5). This linear regression model yields an R = 0.9995 and an R^2 = 0.9990. Equation (18) is obtained by means of a multiple linear regression, taking as dependent variable the values of column E^{rec}, and as independent variable the values X_1 and X_2 (Table 5). This linear regression model yields an R = 0.9999 and an R^2 = 0.9998.

Some initial conclusions that can be drawn from Equations (17) and (18) are that the amount of ΔE_{est}^{sup} needed to get the vehicle moving again after making a single stop is equivalent to the amount of energy needed to ascend 40 m. In the case of E_{est}^{rec}, his ratio decreases, settling at 25 m of descent to recover the same energy as could be recovered in a single stop. From the proposed estimation analysis, the amount of energy input E_{est}^{sup} and of recoverable energy E_{est}^{rec} can be computed in a simple way for each route at each point, by using the coefficients X_1: number of bus stops per km, and X_2: accumulated difference in altitude per km (m/km). These operations are listed in Table 6 and can be easily computed for any route that can be evaluated for any distance d in km.

Table 6. Results obtained for E_{est}^{sup} and E_{est}^{rec} with the regression model.

UT Line	X_1	X_2	E_{est}^{sup} (MJ)	E_{est}^{rec} (MJ)
1	3.39	17.46	4.93 d	3.36 d
2	3.68	14.51	5.22 d	3.50 d
3	3.27	13.26	4.65 d	3.13 d
4	3.00	14.09	4.32 d	2.93 d
5	3.13	13.09	4.46 d	3.00 d
6	3.14	9.67	4.37 d	2.90 d

Based on the data obtained in Table 6, the construction of a resource optimization strategy is suggested, giving top priority to the renovation of buses covering line 2, since this is where the highest energy recovery per km traveled occurs (3.50 MJ/km). Subsequently, to optimize resources, lines 1, 3, 5, 4 and 6 should be renewed respectively. The results obtained from the analysis are compared as follows: E_{est}^{sup} and E_{est}^{rec} (Phase III, Figure 2), in dashed red and dashed green, respectively, versus the data computed at one-second intervals along the entire path using Equation (15) (E^{sup}) and Equation (16) (E^{rec}) in solid red line and solid green line, respectively. The study is carried out on UT line 1 in the city of Ávila (Figure 5). All the energy values shown in the graph are cumulative. In addition, the elevation profile is added (in blue color and values on the secondary axis).

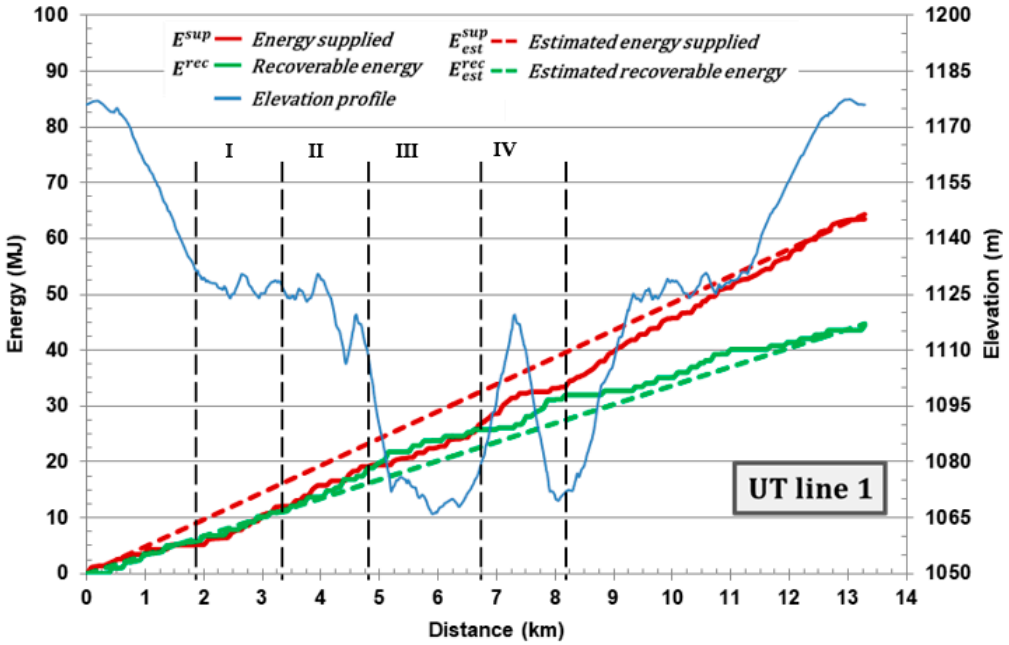


Figure 5. Distribution of Cumulative Energy on line 1 of UT in the city of Ávila (WHS).

From Figure 5, it can be observed that the values of E^{sup}_{est} and E^{rec}_{est}, according to the proposed analysis, follow a straight line with slope according to the corresponding coefficients X_1 and X_2 in Table 5. The values E^{sup} computed according to Equation (15), are far from the estimated values E^{sup}_{est} (decreasing) as the altitude decreases. This is because in the intervals where the accumulated elevation gain is less than the value $X_2 \cdot d$, E^{sup} decreases (less energy needs to be supplied since the vehicle is moving on a negative slope). By the same reasoning, it follows that E^{rec} is greater than the expected E^{rec}_{est} for that interval. Therefore, real values of local accumulated vertical drop that are below the total accumulated vertical drop for a given stretch cause E^{sup} to decrease compared to E^{sup}_{est} and E^{rec} increases compared to E^{rec}_{est}. This behavior can be observed in interval III of Figure 5. The lower the altitude, the more the computed values are farther away from the estimated values. In interval IV (Figure 5) it can be observed that as the altitude increases, the computed values get closer to the estimated values until the maximum relative altitude value, when they move away again. In the final values of the graph, the accumulated elevation gains up to this point coincides with the total accumulated elevation gain of the stretch, and the estimated and calculated values coincide.

Another not-so-obvious trend observed is that, on certain occasions, the two curves of E^{sup} decrease in value with respect to the values for E^{sup}_{est}, which is due to the scarcity of bus stops. In interval I, there are 2 bus stops in a space of 1.3 km, which gives a ratio of 1.5 bus stops/km, far below the coefficient X_1 = 3.39 bus stops/km of the total count of line 1. The scarcity of bus stops in this interval means that very little energy input is needed, and, at the same time, there is very little E^{rec} available. The opposite behavior is found in interval II (Figure 5), where 10 stops are accumulated in 2 km, which establishes a ratio of 5 bus stops/km, higher than the global coefficient X_1 = 3.39 bus stops/km, which makes the computed values of E^{sup} go up again with respect to the estimated values of E^{sup}_{est}. A similar trend is observed with the computed values of E^{rec}, which again rise with respect to their estimated equivalents of E^{rec}_{est}. In the same way that occurs with the "accumulated slope" variable, at the end of the graph (Figures 5 and 6a), the accumulated values coincide with the value of the interval, obtaining computed values very close to those of the estimated model.

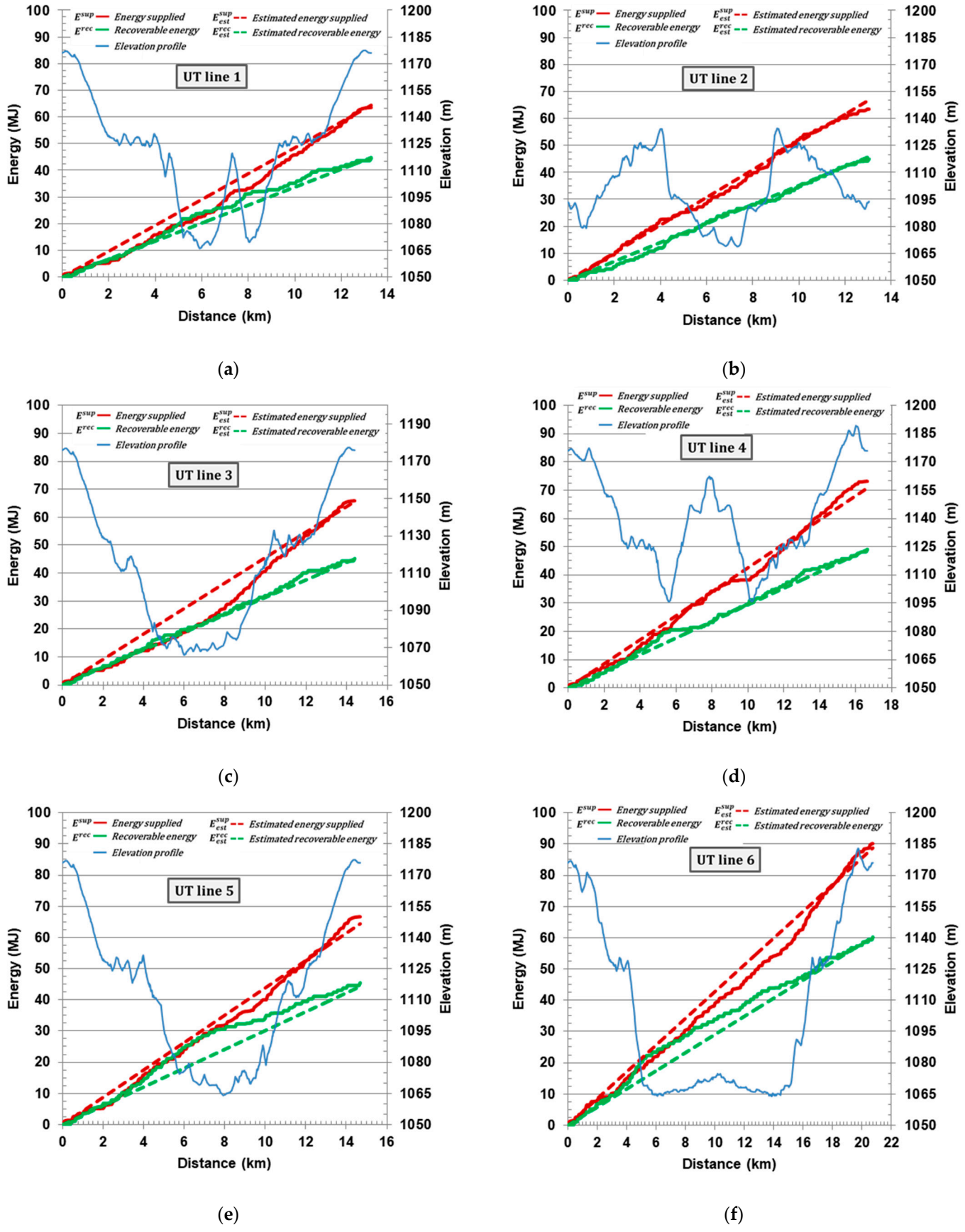


Figure 6. Distribution of accumulated energy in the different UT lines in the city of Ávila (WHS): (**a**) Line 1; (**b**) Line 2; (**c**) Line 3; (**d**) Line 4; (**e**) Line 5; and (**f**) Line 6.

In the case of Line 2 (Figure 6b) it starts with an ascent from km 0 to km 4, which makes the values of E^{sup} and E^{rec} move away from each other and symmetrically to the bisector of the lines E^{r}_{est} and E^{rec}_{est}. From km 4 to km 7.5 the line profile is descending and the values of E^{sup} and E^{rec} approach each other and symmetrically to the bisector of the E^{sup}_{est} and E^{sup}_{est} lines. The same effects are repeated for the upward interval from 7.5 km to 9 km and for the downward interval from 9 km to 13 km.

In line 3 (Figure 6c), a heretofore unseen phenomenon is observed. In the interval from 0 km to 9 km there is a very considerable drop of E^{sup} versus E^{sup}_{est} without a similar displacement of E^{rec} versus E^{rec}_{est}. This is because in that 0–9 km interval there is a conjunction of two factors. On the one hand, there is a very steep decline and, on the other hand, very little concentration of bus stops, 2.7 bus stops/km versus 3.27 bus stops/km on the full line 3. This occurs because the vehicle moving at a constant v and down a negative gradient, does not need much E^{sup} to move. However, since there are fewer bus stops in that interval, there is less braking (the event where more E^{rec} can be recovered), so there is no significant increase in E^{rec} versus E^{rec}_{est}. In the interval from 9 km to 13 km the opposite occurs, many bus stops with a positive slope, which causes a large amount of E^{sup} to be needed so that, in this interval E^{sup} again approaches the values of E^{sup}_{est}.

The opposite phenomenon occurs in line 5 (Figure 6e). In this line 5, there is a very steep decline, but, unlike line 3 (Figure 6c), in line 5 there are many bus stops together. The interval 4–6 km, has 4.5 bus stops per km, compared to 3.13 bus stops/km on the entire line 5. By braking many times, the E^{rec} values increase a lot, while an amount of E^{sup} very similar to E^{sup}_{est} must be contributed because the bus has to be accelerated many times. For line 4 (Figure 6d) and line 6 (Figure 6f) a very homogeneous distribution of bus stops is observed, so there is a direct relationship between the slope of the route and the distance of E^{sup} and E^{rec} with respect to their corresponding homologues.

Finally, as can be observed in the six UT lines (Figure 6) of the city of Avila (WHS), there is a variation of the computed energy with respect to the energy estimated by the proposed method. This is due to the fact that, for the computation of E^{sup}_{est} and E^{sup}_{est} according to the proposed numerical model, both the accumulated gradient and the number of bus stops are assumed constant along the entire route, while the computed energy values E^{sup} and E^{rec}, considering the gradient in each one-second interval.

The proposed method can estimate E^{sup}_{est} and E^{sup}_{est} assuming a constant accumulated gradient and a constant number of bus stops. This means that the proposed method will yield results of E^{sup}_{est} and E^{sup}_{est} very similar to E^{sup} and E^{rec} respectively, if the studied interval has values of X_1 and X_2 similar to those of a given run. The main difference is between the local values of X_1 and X_2 with respect to the global values of the considered path, this difference being greater the further the estimated energy values are from the calculated values.

The present study is oriented to the replacement of old fuel buses by new hybrid or fully electric buses, so energy units are taken, which are valid for any type of buses. In this sense, from the proposed method it is possible to make an energy study to classify the lines where there is the greatest possibility of energy use, allowing to generate strategies in the renovation of buses that allow better use of energy resources. On the other hand, the method is not able by itself to optimize the energy consumption, but it is only able to analyze the energy consumption of the different UT lines. The computation of the energy consumption is then proposed as a future line of research.

As a future research line, it is proposed to focus the study on the construction of a mathematical model for the energy supplied and recovered, by means of a statistical analysis of Bayesian inference, based on Markov Chain Monte Carlo algorithms. This statistical analysis would allow the identification of other variables related to the lines (different to the analyzed in this paper: number of stops, length, and cumulative elevation) that may be influencing the energy supplied and recovered variables, and thus help provide a stochastic model to optimize energy consumption.

5. Conclusions

The urban transport sector is evolving towards sustainability and decarbonization, making ever better use of the energy consumed and achieving efficiency rates never seen before. The way to quickly achieve these efficiency goals in urban passenger transport would be to renew the entire fleet of buses for more modern ones equipped with regenerative braking systems. However, on many occasions, the resources available to local administrations are limited and do not allow for the replacement of an entire fleet of buses, or this replacement must be done progressively over the years. It is in this situation that a thorough understanding of the conditions that contribute most to transport inefficiency is essential.

In the case of World Heritage Sites, such as the present study in the city of Ávila (Spain), knowledge of these conditions can ensure that available resources are directed to where they are most needed, and thus maximize the benefits of investments in public transport. It is not just a matter of investing resources in sustainable transport, but also of ensuring that the resources allocated are put to the best possible use.

One of the ways to achieve the above objectives is to recover as much energy as possible in urban public transport journeys. Thanks to the mathematical model proposed in this research, the recoverable energy per unit of distance traveled by urban buses will be greater the higher the number of accelerations (number of bus stops per km; X_1) and the steeper the landscape (accumulated slope per km; X_2). Therefore, if the driving is done including many of these variables, it will be necessary to implement a regenerative braking system, while, if the driving is done smoothly and on the flat, the benefit of regenerative braking is of little importance.

The mathematical model developed in the present research not only reflects the above statement, but also quantifies in what proportion each of the variables considered contributes to the energy that is necessary to make an urban route and the energy that can be recovered in this route. In addition, the mathematical model developed facilitates the design of urban transport routes in a more efficient way, based on a combination of energy criteria not highlighted to date, such as the estimation of E^{sup} and E^{rec} on the conjunction of two easily obtainable data in any UT route in the world, such as X_1 and X_2.

In addition, this mathematical model allows optimizing the implementation process of regenerative braking systems, ensuring their maximum use, because in the case of a possible partial implementation of regenerative braking systems in a fleet of UT buses, the model allows prioritizing the use of these systems in those places where the greatest use is obtained from them. In the case of the city of Ávila (WHS), the results obtained have made it possible to classify the 6 existing UT lines, clearly establishing a preferential order for replacing older vehicles with new vehicles equipped with regenerative braking. The fact of establishing a method to prioritize the implementation of vehicles with regenerative braking in the lines where more energy can be recovered would lead to a maximum use of energy resources and, therefore, of economic resources, obtaining the highest possible efficiency levels.

Author Contributions: Conceptualization, C.S.-I., P.F.-A. and D.V.; methodology, C.S.-I., P.F.-A. and D.V.; validation, C.S.-I., P.F.-A. and D.V.; formal analysis, C.S.-I., P.F.-A., Á.A.-S. and D.V.; data curation, C.S.-I., P.F.-A. and D.V.; writing—original draft preparation, C.S.-I., P.F.-A., Á.A.-S. and D.V.; writing—review and editing, C.S.-I., P.F.-A., Á.A.-S. and D.V.; supervision, C.S.-I., P.F.-A., Á.A.-S. and D.V. All authors have read and agreed to the published version of the manuscript.

Funding: This research received no external funding.

Institutional Review Board Statement: Not applicable.

Informed Consent Statement: Not applicable.

Conflicts of Interest: The authors declare no conflict of interest.

Abbreviations

Symbol	Variable Description
P_{wind}	Aerodynamic power
F_{wind}	Aerodynamic drag
C_x	Aerodynamic drag coefficient
ρ	Air density
X_2	Cumulative elevation gains per km
d	Distance
g	Earth gravity acceleration
r	Earth radius
$E_{\text{est}}^{\text{sup}}$	Estimated supplied energy
$E_{\text{est}}^{\text{rec}}$	Estimated recoverable energy
A_{f}	Frontal area
P_{grad}	Grading power
F_{grad}	Grading drags
H	Height
ΔE_C	Increased kinetic energy
IP	Instantaneous power
φ_1, φ_2	Latitude of point 1 and latitude of point 2
λ_1, λ_2	Longitude of point 1 and longitude of point 2
MRO	Mass in running order
MAM	Maximum authorized mass
pax	Number of passengers
X_1	Number of bus stops per km
P^{sup}	Supplied power
P^{rec}	Recoverable power
P_{roll}	Rolling power
F_{roll}	Rolling drag
fr	Rolling drag coefficient
S	Separation between two points
α	Slope angle
E^{sup}	Supplied energy
m	Vehicle mass
v	Velocity
W	Width
v_{w}	Wind velocity

References

1. Gkoumas, K.; Marques, F.L.; Stepniak, M.; Pekár, F. Research and Innovation Supporting the European Sustainable and Smart Mobility Strategy: A Technology Perspective from Recent European Union Projects. *Appl. Sci.* **2021**, *11*, 11981. [CrossRef]
2. Von Homeyer, I.; Oberthür, S.; Jordan, A.J. EU climate and energy governance in times of crisis: Towards a new agenda. *J. Eur. Public Policy* **2021**, *28*, 959–979. [CrossRef]
3. Ossewaarde, M.; Ossewaarde-Lowtoo, R. The EU's Green Deal: A Third Alternative to Green Growth and Degrowth? *Sustainability* **2020**, *12*, 9825. [CrossRef]
4. Rhodes, C.J. The 2015 Paris Climate Change Conference: COP21. *Sci. Prog.* **2016**, *99*, 97–104. [CrossRef] [PubMed]
5. Pietrzak, M.B.; Olczyk, M.; Kuc-Czarnecka, M.E. Assessment of the Feasibility of Energy Transformation Processes in European Union Member States. *Energies* **2022**, *15*, 661. [CrossRef]
6. Tian, J.; Yu, L.; Xue, R.; Zhuang, S.; Shan, Y. Global low-carbon energy transition in the post-COVID-19 era. *Appl. Energy* **2022**, *307*, 118205. [CrossRef]
7. Pakulska, T. Green Energy in Central and Eastern European (CEE) Countries: New Challenges on the Path to Sustainable Development. *Energies* **2021**, *14*, 884. [CrossRef]
8. Quintana-Rojo, C.; Callejas-Albiñana, F.-E.; Tarancón, M.-Á.; Martínez-Rodríguez, I. Econometric Studies on the Development of Renewable Energy Sources to Support the European Union 2020–2030 Climate and Energy Framework: A Critical Appraisal. *Sustainability* **2020**, *12*, 4828. [CrossRef]
9. Kulovesi, K.; Oberthür, S. Assessing the EU's 2030 Climate and Energy Policy Framework: Incremental Change toward Radical Transformation? *Rev. Eur. Comp. Int. Environ. Law* **2020**, *29*, 151–166. [CrossRef]

10. Wójcik-Jurkiewicz, M.; Czarnecka, M.; Kinelski, G.; Sadowska, B.; Bilińska-Reformat, K. Determinants of Decarbonisation in the Transformation of the Energy Sector: The Case of Poland. *Energies* **2021**, *14*, 1217. [CrossRef]
11. Calise, F.; Fabozzi, S.; Vanoli, L.; Vicidomini, M. A sustainable mobility strategy based on electric vehicles and photovoltaic panels for shopping centers. *Sustain. Cities Soc.* **2021**, *70*, 102891. [CrossRef]
12. Gössling, S.; Cohen, S. Why sustainable transport policies will fail: EU climate policy in the light of transport taboos. *J. Transp. Geogr.* **2014**, *39*, 197–207. [CrossRef]
13. Pamuła, T.; Pamuła, W. Estimation of the Energy Consumption of Battery Electric Buses for Public Transport Networks Using Real-World Data and Deep Learning. *Energies* **2020**, *13*, 2340. [CrossRef]
14. Kim, J.; Song, I.; Choi, W. An Electric Bus with a Battery Exchange System. *Energies* **2015**, *8*, 6806–6819. [CrossRef]
15. Abdelaty, H.; Mohamed, M. A Prediction Model for Battery Electric Bus Energy Consumption in Transit. *Energies* **2021**, *14*, 2824. [CrossRef]
16. Bottiglione, F.; Contursi, T.; Gentile, A.; Mantriota, G. The Fuel Economy of Hybrid Buses: The Role of Ancillaries in Real Urban Driving. *Energies* **2014**, *7*, 4202–4220. [CrossRef]
17. Pojani, D.; Stead, D. Sustainable Urban Transport in the Developing World: Beyond Megacities. *Sustainability* **2015**, *7*, 7784–7805. [CrossRef]
18. Goldman, T.; Gorham, R. Sustainable urban transport: Four innovative directions. *Technol. Soc.* **2006**, *28*, 261–273. [CrossRef]
19. Sánchez-Chóliz, J.; Duarte, R. CO_2 emissions embodied in international trade: Evidence for Spain. *Energy Policy* **2004**, *32*, 1999–2005. [CrossRef]
20. Alcántara, V.; Roca, J. Energy and CO_2 emissions in Spain: Methodology of analysis and some results for 1980–1990. *Energy Econ.* **1995**, *17*, 221–230. [CrossRef]
21. Ministry for Ecological Transition and the Demographic Challenge. Transport Sector. Available online: https://www.miteco.gob.es/es/cambio-climatico/temas/mitigacion-politicas-y-medidas/transporte.aspx (accessed on 11 January 2022).
22. Navas-Anguita, Z.; García-Gusano, D.; Iribarren, D. Long-term production technology mix of alternative fuels for road transport: A focus on Spain. *Energy Convers. Manag.* **2020**, *226*, 113498. [CrossRef] [PubMed]
23. Junta de Castilla y León. Regional Strategy against Climate Change in Castilla and León 2009–2012–2020. Available online: https://medioambiente.jcyl.es/web/jcyl/MedioAmbiente/es/Plantilla100Detalle/1246988359553/Programa/1284497829991/Comunicacion (accessed on 14 January 2022).
24. Martín-Viso, I. Commons and the construction of power in the early Middle Ages: Tenth-century León and Castile. *J. Mediev. Hist.* **2020**, *46*, 1–23. [CrossRef]
25. United Nations Educational, Scientific and Cultural Organization. World Heritage List. Available online: https://whc.unesco.org/en/list/ (accessed on 4 January 2022).
26. Bigio, A.G.; Ochoa, M.C.; Amirtahmasebi, R. *Climate-Resilient, Climate-Friendly World Heritage Cities*; Urban Development Series; The World Bank Group: Washington, DC, USA, 2014.
27. Gullino, P.; Beccaro, G.L.; Larcher, F. Assessing and Monitoring the Sustainability in Rural World Heritage Sites. *Sustainability* **2015**, *7*, 14186–14210. [CrossRef]
28. Ramos-Soler, I.; Martínez-Sala, A.-M.; Campillo-Alhama, C. ICT and the Sustainability of World Heritage Sites. Analysis of Senior Citizens' Use of Tourism Apps. *Sustainability* **2019**, *11*, 3203. [CrossRef]
29. May, A.D. Urban Transport and Sustainability: The Key Challenges. *Int. J. Sustain. Transp.* **2013**, *7*, 170–185. [CrossRef]
30. Lin, C.-L.; Hung, H.-C.; Li, J.-C. Active Control of Regenerative Brake for Electric Vehicles. *Actuators* **2018**, *7*, 84. [CrossRef]
31. Zhao, X.; Li, L.; Wang, X.; Mei, M.; Liu, C.; Song, J. Braking force decoupling control without pressure sensor for a novel series regenerative brake system. *Proc. Inst. Mech. Eng. Part D J. Automob. Eng.* **2019**, *233*, 1750–1766. [CrossRef]
32. Cai, J.W.; Chu, L.; Fu, Z.C.; Ren, L.P. Regenerative Braking System for a Pure Electric Bus. *Appl. Mech. Mater.* **2014**, *543–547*, 1405–1408. [CrossRef]
33. Han, T.; Zeng, B.; Tong, Y. Theoretical study on energy recovery rate of regenerative braking for hybrid mining trucks with different parameters. *J. Energy Storage* **2021**, *42*, 103127. [CrossRef]
34. Yadav, D.; Kumar, R.; Kulshrestha, U.; Jain, A.; Rani, S. Enhancement of fuel efficiency in heavy duty vehicles through integrated module of TEG, piezoelectric and regenerative braking solutions. *Mater. Today Proc.* 2021, in press. [CrossRef]
35. Ghafouryan, M.M.; Ataee, S.; Dastjerd, F.T. A novel method for the design of regenerative brake system in an urban automotive. *J. Braz. Soc. Mech. Sci. Eng.* **2016**, *38*, 945–953. [CrossRef]
36. Ma, Z. Parameters design for a parallel hybrid electric bus using regenerative brake model. *Adv. Mech. Eng.* **2014**, *6*, 760815. [CrossRef]
37. Xiao, B.; Lu, H.; Wang, H.; Ruan, J.; Zhang, N. Enhanced Regenerative Braking Strategies for Electric Vehicles: Dynamic Performance and Potential Analysis. *Energies* **2017**, *10*, 1875. [CrossRef]
38. Avanza Spain, S.L.U. Plano de las Líneas de la Ciudad de Ávila. Available online: https://avila.avanzagrupo.com/lineas-y-horarios/plano-de-las-lineas (accessed on 11 March 2022).
39. Zhao, P.; Haitao, H.; Li, A.; Mansourian, A. Impact of data processing on deriving micro-mobility patterns from vehicle availability data. *Transp. Res. Part D Trans. Environ.* **2021**, *97*, 102913. [CrossRef]
40. Whang, F.; Chen, C. On data processing required to derive mobility patterns from passively-generated mobile phone data. *Transp. Res. Part C Emerg. Tech.* **2018**, *87*, 58–74. [CrossRef]

41. Dauni, P.; Firdaus, M.D.; Asfariani, R.; Saputra, M.I.N.; Hidayat, A.A.; Zulfikar, W.B. Implementation of Haversine formula for school location tracking. *J. Phys. Conf. Ser.* **2019**, *1402*, 077028. [CrossRef]
42. Baure, G.; Dubarry, M. Synthetic vs. Real driving cycles: Baure, G.; Dubarry, M. Synthetic vs. Real Driving Cycles: A Comparison of Electric Vehicle Battery Degradation. *Batteries* **2019**, *5*, 42. [CrossRef]
43. Huzayyin, O.A.; Salem, H.; Hassan, M.A. A representative urban driving cycle for passenger vehicles to estimate fuel consumption and emission rates under real-world driving conditions. *Urban Clim.* **2021**, *36*, 100810. [CrossRef]
44. Cui, Y.; Xu, H.; Zou, F.; Chen, Z.; Gong, K. Optimization based method to develop representative driving cycle for real-world fuel consumption estimation. *Energy* **2021**, *235*, 121434. [CrossRef]
45. Mercedes Benz Bus. Available online: https://www.mercedes-benz-bus.com/es_ES/models/citaro/facts/technical-data.html (accessed on 14 February 2022).
46. Humanetics. Available online: https://humanetics.humaneticsgroup.com/products/anthropomorphic-test-devices/frontal-impact/hybrid-iii-50th-male/hybrid-iii-50th-male (accessed on 14 February 2022).
47. Ehsani, M.; Gao, Y.; Gay, S.E.; Emadi, A. *Modern Electric, Hybrid Electric, and Fuel Cell Vehicles*; CRC Press: Boca Raton, FL, USA, 2005; pp. 21–29.
48. Greenwood, J.A.; Minshall, H.; Tabor, D. Hysteresis losses in rolling and sliding friction. *Proc. R. Soc. London. Ser. A. Math. Phys. Sci.* **1961**, *259*, 480–507. [CrossRef]
49. Komandi, G. An evaluation of the concept of rolling drag. *J. Terramechanics* **1999**, *36*, 159–166. [CrossRef]
50. Rill, G. *Road Vehicle Dynamics. Fundamentals and modeling*; CRC Press: Boca Raton, FL, USA, 2012; pp. 225–227.
51. Guiggiani, M. *The Science of Vehicle Dynamics. Handling, Braking, and Ride of Road and Race Cars*; Springer: Dordrecht, The Netherlands; Heidelberg, Germany; New York, NY, USA, 2014; pp. 59–61.
52. Lin, N.; Zong, C.; Shi, S. The method of mass estimation considering system error in vehicle longitudinal dynamics. *Energies* **2019**, *12*, 52. [CrossRef]
53. Koreny, M.; Simonik, P.; Klein, T.; Mrovec, T.; Ligori, J.J. Hybrid research platform for fundamental and empirical modeling and analysis of energy management of shared electric vehicles. *Energies* **2022**, *15*, 1300. [CrossRef]
54. Guerrero, A.; Castilla, R.; Eid, G. A Numerical aerodynamic analysis on the effect of rear underbody diffusers on road cars. *Appl. Sci.* **2022**, *12*, 3763. [CrossRef]
55. Luján, J.M.; Piqueras, P.; de la Morena, J.; Redondo, F. experimental characterization of real driving cycles in a light-duty diesel engine under different dynamic conditions. *Appl. Sci.* **2022**, *12*, 2472. [CrossRef]
56. Kaluva, S.T.; Pathak, A.; Ongel, A. Aerodynamic drag analysis of autonomous electric vehicle Platoons. *Energies* **2020**, *13*, 4028. [CrossRef]